Comparison of OCO-2 target observations to MUCCnet - Is it possible to capture urban X_{CO2} gradients from space?

Maximilian Rißmann[1], Jia Chen[1], Gregory Osterman[2], Xinxu Zhao[1], Florian Dietrich[1], Moritz Makowski[1], Frank Hase[3], and Matthäus Kiel[2]

[1]Environmental Sensing and Modeling, Technical University of Munich (TUM), Munich, Germany
[2]Jet Propulsion Laboratory, California Institute of Technology, Pasadena, CA, USA
[3]Institute of Meteorology and Climate Research (IMK-ASF), Karlsruhe Institute of Technology (KIT), Karlsruhe, Germany

Correspondence: Jia Chen (jia.chen@tum.de)

Abstract.

In this paper, we compare Orbiting Carbon Observatory 2 (OCO-2)'s measurements of column-averaged dry air mole fractions (DMF) of CO_2 (X_{CO2}) and its urban-rural differences against ground-based remote sensing data measured by the Munich Urban Carbon Column network (MUCCnet). Since April 2020, OCO-2 regularly conducts target observations in Munich, Germany. Its target mode data provides high resolution X_{CO2} within a $15\,km \times 20\,km$ target field-of-view, that is greatly suited for carbon emission studies from space in cities and agglomerated areas. OCO-2 detects urban X_{CO2} with a RMSD of less than 1 ppm when compared to the MUCCnet reference site. OCO-2 target X_{CO2} is biased high against the ground-based measurements. The close proximity of MUCCnet's five fully automated remote sensing sites enables us to compare space-borne and ground-based X_{CO2} in three urban areas of Munich separately (centre, north, and west), by dividing the target field into three smaller comparison domains. Due to this more constrained collocation, we observe improved agreement between space-borne and ground-based X_{CO2} in all three comparison domains.

For the first time, X_{CO2} gradients within one OCO-2 target field-of-view are evaluated against ground-based measurements. We compare X_{CO2} gradients in the OCO-2 target observations to gradients captured by collocated MUCCnet sites. Generally, OCO-2 detects elevated X_{CO2} in the same regions as the ground-based monitoring network. More than 90% of the observed space-borne gradients have the same orientation as the X_{CO2} gradients measured by MUCCnet. During our study, urban-rural enhancements are found to be in the range of 0.1 to 1 ppm. The low urban-rural gradients of typically well below 1 ppm in Munich during our study allow us to test OCO-2's lower detection limits for intra-urban X_{CO2} gradients. Urban X_{CO2} gradients recorded by the OCO-2 instruments and MUCCnet are strongly correlated ($R^2 = 0.68$) with each other and have an RMSD of 0.32 ppm. A case study, which includes a comparison of one OCO-2 target overpass to WRF-GHG modeled X_{CO2}, reveals a similar distribution of enhanced CO_2 column abundances in Munich. In this study, we address OCO-2's capability of detecting small-scale spatial X_{CO2} differences within one target observation. Our results suggest OCO-2's potential of assessing anthropogenic emissions from space.

1 Introduction

Constantly rising atmospheric mole fractions of greenhouse gases, such as carbon dioxide (CO_2) and methane (CH_4), make
combating climate change to mankind's most urgent global challenge. Even though, stringent climate targets were formulated
under the 2015 Paris Agreement aimed to limit the temperature increase to well below 2 °C, still rising anthropogenic emission
causes global mean temperatures to surge to record highs resulting in a growing number of severe and fatal weather events, that
can be linked to climate change (Shukla et al., 2019). The Annual Greenhouse Gas Index (AGGI), which is a measure for the
radiative forcing of all anthropogenic greenhouse gases (GHGs) combined, reached an all time high of 1.47 in 2021, indicating
a 47 % increase in total radiative forcing since 1990 due to rising GHG mole fractions. Especially problematic is the atmo-
spheric surge of CO_2, which contributes about 80 % of this growth in radiative forcing (Montzka, 2021). Emissions from urban
areas play a key role in this development as they are responsible for more than 70 % of global manmade GHG emissions, even
though they cover less than 3 % of land area globally (Wu et al., 2016; Gurney et al., 2015). These numbers illustrate the impor-
tance of long-term observations of CO_2 mole fractions, especially in large and middle sized cities as well as closely monitoring
short term X_{CO2} fluxes on a sub-city scale, which gives insights on anthropogenic emission and can provide policy makers with
the information needed to enact more efficient and improved emission reduction policies. The Total Column Carbon Observing
Network (TCCON) is a global network of Fourier Transform Infrared (FTIR) spectrometers of the type Bruker IFS 125HR at
25 sites in a multitude of longitudinal and latitudinal zones (Wunch et al., 2011). It monitors the long-term atmospheric growth
of XCO2, XCO and XCH4 along with other atmospheric trace gases. Regular calibrations against aircraft measurements make
the TCCON sites currently the primary validation source for most space-based X_{CO2} data products (GOSAT, GOSAT-2, OCO-
3, TROPOMI). Other ground-based networks like the Collaborative Carbon Column Observing Network (COCCON) aim to
improve spatial coverage by operating the low cost and portable Bruker EM27/SUN spectrometers, which are also well suited
as ground-based references for OCO-2 validation efforts (Jacobs et al., 2020; Frey et al., 2019).

In recent years, EM27/SUN instruments have been used in measurement campaigns that aim to quantify urban anthropogenic
emissions by combining differential column measurements (DCM) and atmospheric transport models (Chen et al., 2016). Mul-
tiple field campaigns have been carried out in Berlin (Hase et al., 2015), Munich (Dietrich et al., 2021), Indianapolis (Jones
et al., 2021), Poland (Luther et al., 2019, 2021), Chino (Chen et al., 2016), St. Petersburg (Makarova et al., 2021) and Ham-
burg (Chen et al., 2022). These studies show the potential of top-down emission estimates as they can help uncover unknown
emission sources and constrain bottom-up emission inventories.

In addition to the increasing number of ground-based instruments, the constantly improving space-borne remote sensing sys-
tems drastically enhance the global coverage of precise X_{CO2} measurements even in hard to reach, solitary areas. NASA's
Orbiting Carbon Observatory instruments (OCO-2 and OCO-3) capture X_{CO2} in four different measurements modes: nadir,
glint, target and snapshot area mode (SAM). OCO-2 captures X_{CO2} on a 16-day ground-track repeat cycle (Osterman et al.,
2020). Previous studies investigated urban to rural X_{CO2} enhancements (Park et al., 2021) and extracted CO_2 emission signals
from OCO-2 nadir tracks (Wu et al., 2018; Shekhar et al., 2020). Recently, Kiel et al. (2021) compared OCO-3 SAM and target
observations over the Los Angeles Mega city against simulated X_{CO2} from two different models. This study showed that spa-
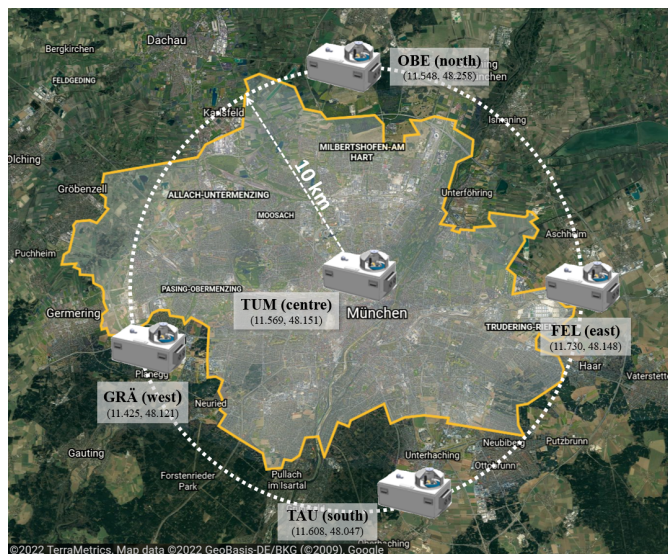
Figure 1. Locations of EM27/SUN spectrometers in Munich. The centre site is located on the roof of the TUM building in Munich. The other spectrometers are distributed around Munich in each compass direction.

tially fine scale satellite measurements have the potential to resolve X_{CO2} differences on a sub-city scale. Even though OCO-2 and OCO-3 measurements are evaluated against TCCON observations on a regular basis, these comparisons are performed on a global scale and do not provide information about OCO-2's data quality on sub-city scales. In this study, for the first time,

60 we test OCO-2's capability to determine sub-city X_{CO2} differences within one target field (approx. 15 x 20 km) by comparing OCO-2 target soundings against measurements of the Munich Urban Column Concentration network (MUCCnet). MUCCnet is a novel, fully automated ground-based network that continuously measures CO_2, CH_4 and CO column concentrations at its five sites in and around Munich (Dietrich et al., 2021). The close proximity of the ground-based instruments allows us to compare absolute OCO-2 X_{CO2} in different parts of Munich and also lets us evaluate space-borne X_{CO2} enhancements. This

65 way, we test the capability of OCO-2 to resolve small-scale urban X_{CO2} fluxes in Munich and other cities from space, which is needed to study sector dependent emissions in the future. Due to OCO-2's relatively small target size of around 300 square kilometers the instrument is best suited for spaceborne emission studies in smaller cities while OCO-3's SAM measurements cover a wider field-of-view, which enables the assessment of larger agglomerated areas (Kiel et al., 2021).

2 Datasets

70 ### 2.1 MUCCnet X_{CO2} data

The solar spectra that are acquired by the five MUCCnet EM27/SUN devices are evaluated by two retrieval algorithms (Dietrich et al., 2021): GGG2014 (Wunch et al., 2011) and PROFFAST (Frey et al., 2019; Alberti et al., 2022). In this study, we

consider the X_{CO2} outputs of the PROFFAST retrieval algorithm (Hase et al., 2004; Frey et al., 2015) that fits atmospheric CO_2 by scaling a priori column profiles to match the solar spectra measured by the spectrometers (Frey et al., 2019). The software

75   is developed and maintained by the Karlsruhe Institute of Technology (KIT). The PROFFAST algorithm considers the Instrumental Line Shapes (ILS) of the individual EM27/SUN devices to reduce systematic instrument specific errors in the trace gas retrieval (Frey et al., 2015; Alberti et al., 2022). The ILS parameters, phase error (PE) and modulation efficiency (ME) of the instruments at the maximum optical path length (OPD_{max}) as derived from open path measurements under controlled ambient conditions (Frey et al., 2019). The instrument-specific ILS parameters as resulting from the open path calibrations are stored in

80   the spectra generated with the PROFFAST preprocessor and are subsequently used in the trace gas analysis (Gisi et al., 2012; Sha et al., 2020).

The remaining instrument- and gas-specific discrepancies are determined by analysing side-by-side solar observations performed at the calibration facility of the COllaborative Carbon Column Observation Network (Frey et al., 2019). A reference COCCON instrument (serial number SN37) and a collocated TCCON spectrometer in Karlsruhe serve as standard of compar-

85   ison. The resulting empirical corrections summarize all remaining unexplained instrument-specific corrections and are applied as instrument specific calibration factors K_{XCO2}^{SN} on the raw X_{CO2}^{raw} values generated by the PROFFAST retrieval code:

$$X_{CO2}^{scaled} = K_{XCO2}^{SN} \cdot X_{CO2}^{raw} . \qquad (1)$$

This indirectly ties the MUCCnet X_{CO2} retrievals to the TCCON site in Karlsruhe since the COCCON reference device is calibrated against the TCCON site in Karlsruhe (Alberti et al., 2022; Frey and Gisi, 2021). Each MUCCnet spectrometer is pro-

90   tected by an enclosure, which is equipped with a multitude of sensors to fully automate the retrieval process (Heinle and Chen, 2018; Dietrich et al., 2021). Among others, the enclosures are equipped with a low cost air pressure sensor (Model 61302, Young (2009)) that captures the ground-pressure inputs for the PROFFAST retrieval. The pressure sensor of the MUCCnet centre site (TUM) is used to calibrate the other four in-situ pressure sensors. The sensors are calibrated by subtracting constant offsets which are determined in side-by-side measurements. Pressure calibration offsets, instrument specific calibration factors

95   and the ILS parameters are listed in Table 1.

Serial Number (SN)	Location	Longitude (degree)	Latitude (degree)	ME	PE (rad)	K_{CO2}	Δp (hPa)
61	TUM_I	11.569	48.151	0.9830	0.0013	0.9993	0.00
86	FEL	11.73	48.148	0.9830	0.0031	1.00242	-0.2686
115	GRÄ	11.425	48.121	0.9837	0.0024	0.999786	0.0953
116	OBE	11.548	48.258	0.9875	0.0044	0.999973	0.2621
117	TAU	11.608	48.047	0.9791	0.0038	1.000220	0.4656

Table 1. Enclosure positions and EM27/SUN input parameters, that are used for calibrating PROFFAST outputs of the five MUCCnet measurement sites. (Frey and Gisi, 2021; Dietrich et al., 2021)

A global post-correction factor, that depends on the solar zenith angle (SZA), is applied to remove an erroneous low bias in the order of 0.5 ppm in the X_{CO2} retrieval outputs of the current PROFFAST version (Dubravica and Hase (2021), distributed before December, 2021). The following formula removes the low bias in the scaled X_{CO2} retrievals:

$$X_{CO2}^{corrected} = \left[1.0018 - (SZA/90°)^2\right] \cdot X_{CO2}^{scaled} . \tag{2}$$

We tested how this post-processing correction (see Eq. 2) impacts our X_{CO2} validation results. We found that applying the post-correction to the PROFFAST retrieval effectively reduced the bias between MUCCnet and OCO-2. Hence, we can confirm that the preliminary measure is effective and should be used with PROFFAST outputs of the current software version. (Dubravica and Hase, 2021). The X_{CO2} post correction will be removed in the new version of PROFFAST, which already is available to users as a beta version.

The PROFFAST retrieval and calibration process for individual devices ties the data to the COCCON network and via its connection to TCCON it shares TCCON's WMO X2007 trace gas scale (Frey and Gisi, 2021). All results of this paper are based on the scaled and bias-corrected retrievals $X_{CO2}^{corrected}$.

2.2 OCO-2 X_{CO2} data

The OCO-2 instrument was developed by NASA and launched into space on July 2nd, 2014. It orbits the earth as part of the Afternoon satellite train (A-train) at an altitude of 705 km (Crisp, 2011). Its instruments capture solar radiance spectra in one of three observational modes: nadir, glint and target mode. During OCO-2 target observations the instrument scans a certain area of interest, which is around 15 x 20 km in size. To maximize the number of soundings during one overpass the instruments scans the target area for approximately 2 minutes. The instrument captures eight spatially separated footprints simultaneously every 1/3 of a second, theoretically yielding around 4000 measurements per overpass (Crisp, 2011). One 1.29 x 2.29 km OCO-2 footprint covers an area of just under 3 km^2 (Osterman et al., 2020).

The captured solar radiance spectra are processed by the Atmospheric Carbon Observations from Space (ACOS) retrieval software. In this work we use the OCO-2 lite files that are processed with the latest version (v10) of the ACOS retrieval algorithm (O'Dell et al., 2018; Kiel et al., 2019). The corresponding files are publicly available and can be downloaded through the NASA Goddard Earth Science Data and Information Services Center (GES DISC, 2021). Footprint related biases and parametric biases are removed for X_{CO2} retrievals in the OCO-2 lite files. A comprehensive overview of the OCO-2 and OCO-3 data products and the bias correction procedure is given in Osterman et al. (2020). Furthermore, a global scaling factor, derived from regular comparisons of OCO-2 target observations and 29 collocated TCCON sites, is applied to the X_{CO2} lite file data. This ties the OCO-2 lite X_{CO2} to the standard trace scale for atmospheric X_{CO2} of the World Meterology Organisation (WMO scale) (Wunch et al., 2017; Osterman et al., 2017). The most recent comparisons of fully bias corrected OCO-2 target X_{CO2} and TCCON reveals a superb agreement ($rms = 0.86$ ppm, $R^2 = 0.97$) (Kiel, 2021). The data product contains a binary quality flag which flags low quality X_{CO2} soundings ($qf = 1$). In the following, we solely consider good quality X_{CO2} retrievals
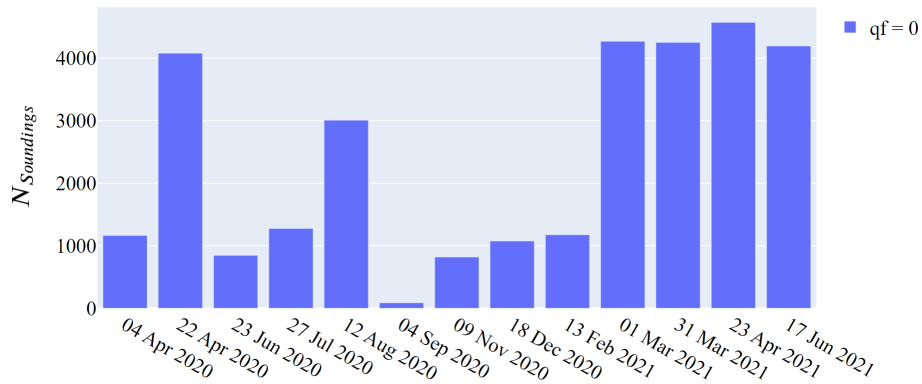
Figure 2. Number of soundings for each of the OCO-2 target overpasses. On most days OCO-2 captured more than 1000 good quality ($qf = 0$) soundings per overpass. Usually a higher number of good quality soundings corresponds with more robust and less sparse data. Thus, we remove overpasses with less than 500 good quality soundings.

130   ($qf = 0$) (Osterman et al., 2020).

The results of this study are based on OCO-2 target observations that took place in recent years, starting from April, 2020. From April 2020 to July 2021 OCO-2 successfully targeted MUCCnet twelve times. Figure 2 summarizes the target dates and the corresponding number of good quality ($qf = 0$) soundings. We include a target observation in our study if 1) the OCO-2

135   instrument gathers a minimum of 500 good quality soundings during the overpass and 2) there are ground-based retrievals for at least one of the three sites within the target field of view. In comparison to other space-borne remotely sensed data products, the relatively small size of the OCO-2 footprints results in a higher number of good quality soundings per target observation even in cloudy conditions. One overpass, which took place on September 4th, 2020, is removed from the comparison set, since only 86 good quality X_{CO2} soundings are retrieved. All remaining days had at least 800 good quality soundings. Figure 3 shows

140   the OCO-2 X_{CO2} observations of the remaining 12 *successful* overpasses over Munich. Due to OCO-2's sun-synchronous orbit, target overpasses in Munich usually take place around 12:00 (UTC). A typical distribution of soundings is shown in Fig. 4. Three of the five MUCCnet sites are within the target field-of-view. Thus, we can compare OCO-2 X_{CO2} against collocated ground-based data in the center (TUM), north (Oberschleißheim) and west (Gräfelfing) of Munich.
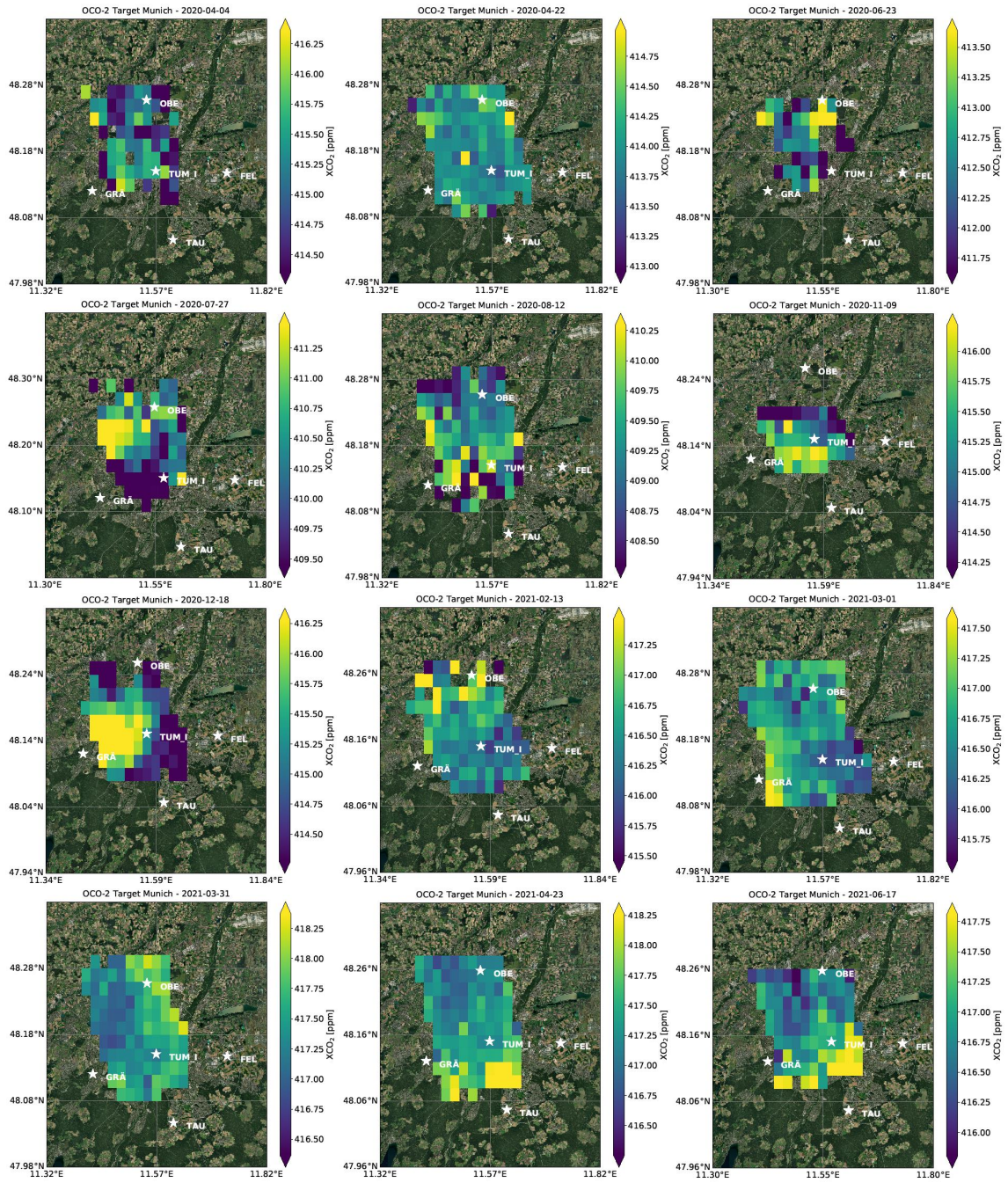
Figure 3. Daily X_{CO2} maps of OCO-2 target observations in Munich. MUCCnet spectrometer locations are highlighted on the map. The OCO-2 target mode data is binned into $0.02° \times 0.02°$ latitude-longitude grid cells. Map Source: Esri, Maxar, Earthstar Geographics, and the GIS User Community
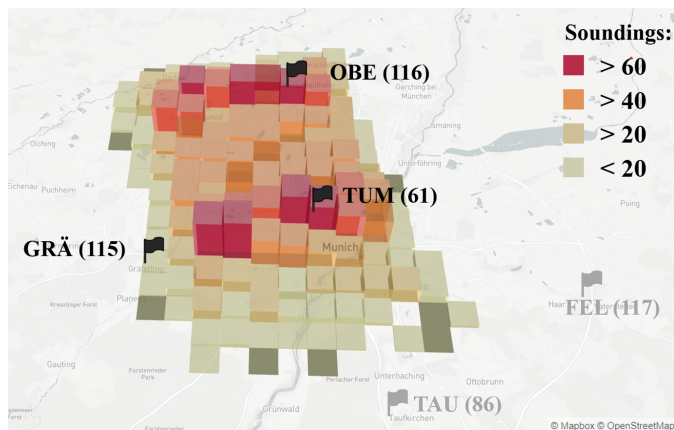
Figure 4. Histogram of OCO-2 target sounding distribution in Munich. There are three MUCCnet sites with sufficient collocated data, which will be considered in this study. Ground-based instruments in Feldkirchen (FEL) and Taufkirchen (TAU) are not featured in this study.

2.3 WRF model setup

We compare the OCO-2 target observations to simulated CO_2 column concentrations, provided by a high-resolution modeling WRF-GHG framework designed for Munich with 45 vertical layers and a horizontal resolution of 400 m (Zhao et al., 2020b). This modeling framework is set up based on the Weather Research and Forecasting model (WRF) coupled with the biospheric flux model (Beck et al., 2011) to quantitatively understand the processes of the emission and consumption of CO_2 and CH_4 in and around Munich. The meteorological initial conditions and lateral boundary conditions in the modelled background concentrations are obtained from the Integrated Forecasting System (IFS) Cycle 47r1, implemented by the European Centre for Medium-Range Weather Forecasts (ECMWF) with a horizontal resolution of approx. 40 km. Near-surface emissions are initialized from the first version of the TNO-GHG and co-emitted species emission database (TNO_GHGco_v1.1; Super et al. (2020)). The details on the model setup and related assessment can be found in Zhao et al. (2020a). X_{CO2} in the study area is derived from the modelled concentration profile u_{mod} which is smoothed with the OCO-2 averaging kernel a, following the method described in O'Dell et al. (2012):

$$XCO_{2,ak} = \sum_{i=1}^{n_{lev}} h_i [a_i u_{mod,i} + (1 - a_i) u_{ap,i}] \,. \tag{3}$$

Here, a_i, h_i and $u_{ap,i}$ denote the ith layer of the normalized averaging kernel vector, the pressure weighting vector and the a priori profile, which can be found in the OCO-2 lite files. The resulting WRF-GHG XCO_2 is binned onto an $0.02° \times 0.02°$ latitude-longitude grid.

3 Methods

3.1 Target Collocation

We use a similar methodology to Wunch et al. (2017) in order to evaluate the OCO-2 X_{CO2} retrievals over Munich against MUCCnet. To compare both data sets we consider the mean of all good quality OCO-2 soundings within the target area and the ground-based X_{CO2} measurements of the MUCCnet centre site $(11.569°E, 48.151°N)$, that have been recorded within ±30 min of the spacecraft's overpass time. Target observations that had less than 500 good quality soundings are not considered in the comparison process. Only the target observation on September 4, 2020 does not meet this requirement.

To account for differences in the MUCCnet and OCO-2 vertical sensitivities, we apply an averaging kernel correction following the approach of Wunch et al. (2011). Hereby, the ground-based X_{CO2} is smoothed with the ACOSv10 column averaging kernel as described in Nguyen et al. (2014). We perform a York regression (York et al., 2004) to determine the best fit line and slope. (Wu and Zhen Yu, 2018).

3.2 By-Site Collocation

Due to the short distance of around 10 km between the MUCCnet instruments, three of the five MUCCnet sites are within the 15x20 km^2 OCO-2 target field-of-view. This lets us evaluate the space-borne X_{CO2} retrievals for different parts of the city. We compare subsets of OCO-2 soundings in each target observation to the X_{CO2} measurements of the closest ground-based instrument.

For a collocation radius of $r_{col} = 6$ km around the spectrometer locations we achieve the highest number of collocated soundings for each site while having almost no overlap of collocated soundings between the sites (most soundings are collocated to only one MUCCnet site). This way, we segment the target observation data into three comparison domains - centre, west and north. A large comparison set of soundings also reduces the effect of random errors in our computed mean X_{CO2}. We assume this relatively large comparison domain to best represent the actual X_{CO2} around our ground-based measurement sites. For each domain we validate space-borne measurements against X_{CO2} data of the collocated MUCCnet spectrometers in Gräfelfing (west, GRÄ), Oberschleißheim (north, OBE) and Munich city centre (centre,TUM). Figure 5 shows the OCO-2 target (taken on March 31, 2021) field-of-view (white square) and the footprint positions of X_{CO2} soundings. The OCO-2 soundings are colour-coded according to their comparison domain (centre = green, west = blue, north = red). The same colour-coding is used for the validation results in section 4.2.

The mean X_{CO2} of OCO-2 soundings in each domain is compared to X_{CO2} measurements of the corresponding MUCCnet site within ±30 min of overpass time. Due to the smaller size of the by-site comparison domains we only consider comparison sets, if 1) at least 70 space-borne soundings are recorded within the collocation area around each MUCCnet site and 2) the collocated ground-based instrument captured at least 50 retrievals within ±30 min of the overpass. On June 17, 2021, we extended the collocation time for the northern site in Gräfelfing to ±60 min, due to sparse ground-based measurements at the exact time of the overpass. The relatively long collocation time frame is chosen due to the low average wind speeds of 2.33 ± 1.54 m/s during the overpasses featured in this study. This may, especially for higher wind speeds, introduce collocation
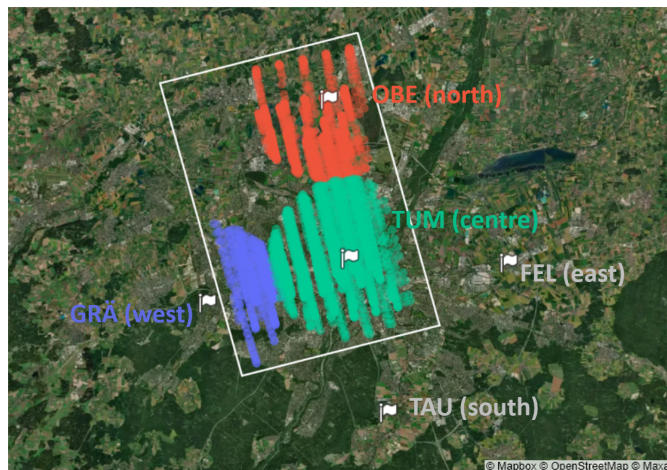
Figure 5. This figure illustrates the collocation criteria for target overpass data captured on March 31, 2021. OCO-2 soundings within a radius of 6 km are compared to measurements of the collocated MUCCnet instrument. The OCO-2 target soundings are coloured according to their collocated ground-based spectrometers.

error which can be reduced by adjusting the collocation time frame according to the wind speed. Figure 6 shows the number
195 of soundings collected by the OCO-2 instruments in each domain N_{domain} for the twelve target observations investigated in this paper.
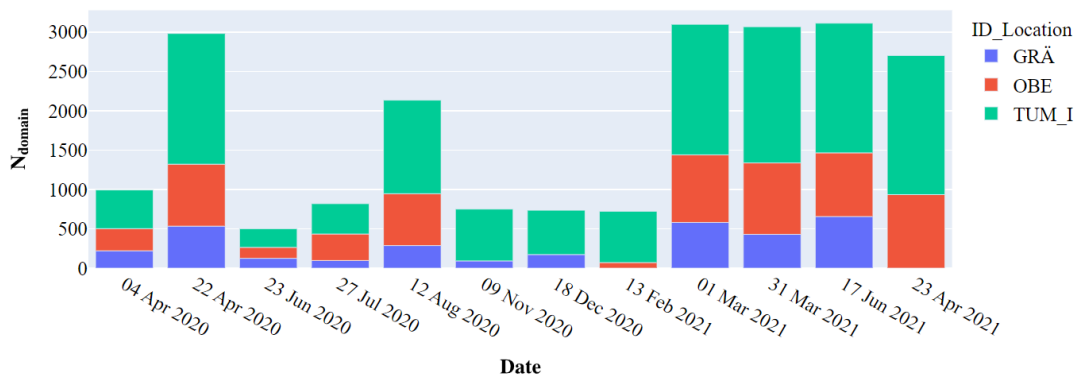
Figure 6. Number of good quality OCO-2 soundings N_{domain} in the three comparison domains.

3.3 Gradient Comparison

We evaluate space-borne X_{CO2} differences in the OCO-2 target field-of-view between the three seperate domains (centre, north and west) against measurements of the collocated MUCCnet spectrometers. We compute the urban gradients, present in the
200 OCO-2 overpasses, by subtracting the mean X_{CO2} of soundings collocated to one of the MUCCnet sites (domain1) from the

mean X_{CO2} of soundings captured in one of the other two comparison areas (domain2):

$$\Delta XCO2_{OCO-2}^{domain1-domain2} = XCO2_{OCO-2}^{domain1} - XCO2_{OCO-2}^{domain2} . \tag{4}$$

This way, we compute three sets of space-borne X_{CO2} gradients that are present in the target observation: 1) west-centre 2) north-centre 3) north-west. Spaceborne X_{CO2} gradients are compared to the X_{CO2} gradients of ground-based measurements of the collocated MUCCnet spectrometers. Ground-based gradients $\Delta XCO2_{MUCCnet}$ are computed by using X_{CO2} data of the collocated MUCCnet sites:

$$\Delta XCO2_{MUCCnet}^{site1-site2} = XCO2_{MUCCnet}^{site1} - XCO2_{MUCCnet}^{site2} . \tag{5}$$

Consequently, X_{CO2} gradients computed between Munich centre and Gräfelfing will also be referred to as "west-centre" gradients, while those between the centre site and Oberschleißheim are called "north-centre" gradients. Positive gradients are obtained if site1 captures higher X_{CO2} than site2. We compute the standard deviation of our gradients between the two domains as follows:

$$SD_{domain1-domain2} = \sqrt{\sigma_{domain1}^2 + \sigma_{domain2}^2} . \tag{6}$$

Rather than the standard error of the mean $SD_{domain1-domain2}$ represents the combined spread of X_{CO2} in the two domains. When compared to the by-site comparison process (Sec. 4.2), we apply stricter criteria to filter which overpasses are considered to be robust and suited for the gradient assessment. We exclude space-borne X_{CO2} gradients, if the mean space-borne X_{CO2} in one of the domains is computed using less than $N_{domain} = 100$ soundings and if it has a standard deviation larger than $\sigma = 0.75$ ppm. This criteria removes two of the gradients from the set (on July 27, 2020 and November 9, 2020). Second, we checked MODIS images taken at overpass time for high cloud coverage. On June 23, the MODIS images and a high aerosol contamination point at challenging measurement conditions causing a sparse distribution of converged soundings around the MUCCnet centre site. Therefore, we do not consider urban X_{CO2} gradients captured on June 23, 2020.

4 Results

4.1 OCO-2 target validation

To test the agreement of OCO-2 and MUCCnet X_{CO2}, we perform a york regression between the twelve OCO-2 target observations and the X_{CO2} measurements of the MUCCnet reference instrument in the centre of the OCO-2 target field-of-view. The results are shown in Fig. 7. For all target observations that are considered in this study, the root mean square X_{CO2} difference is below 1 ppm ($RMSD = 0.96$ ppm). Furthermore, the coefficient of determination $R^2 = 0.93$ reveals a very strong correlation. On average, the space-borne X_{CO2} is about 0.70 ppm higher than the collocated solar measurements taken by the MUCCnet reference device. This high bias is comparable to the observed bias when OCO-2 target data is compared to the Karlsruhe TC-CON instrument (bias= 0.80 ppm, RMSD=0.91) to which MUCCnet is tied (as discussed in Sec. 2.1). The RMSD improves to 0.66 ppm when the bias between the space and ground-based measurements is not taken into account (Matthaeus Kiel, email

correspondence, January 26, 2022). The averaging kernel correction that we applied to the X_{CO2} data improves the root mean square difference by 0.18 ppm. Similar effects of the averaging kernel correction are also observed in Kiel et al. (2021).
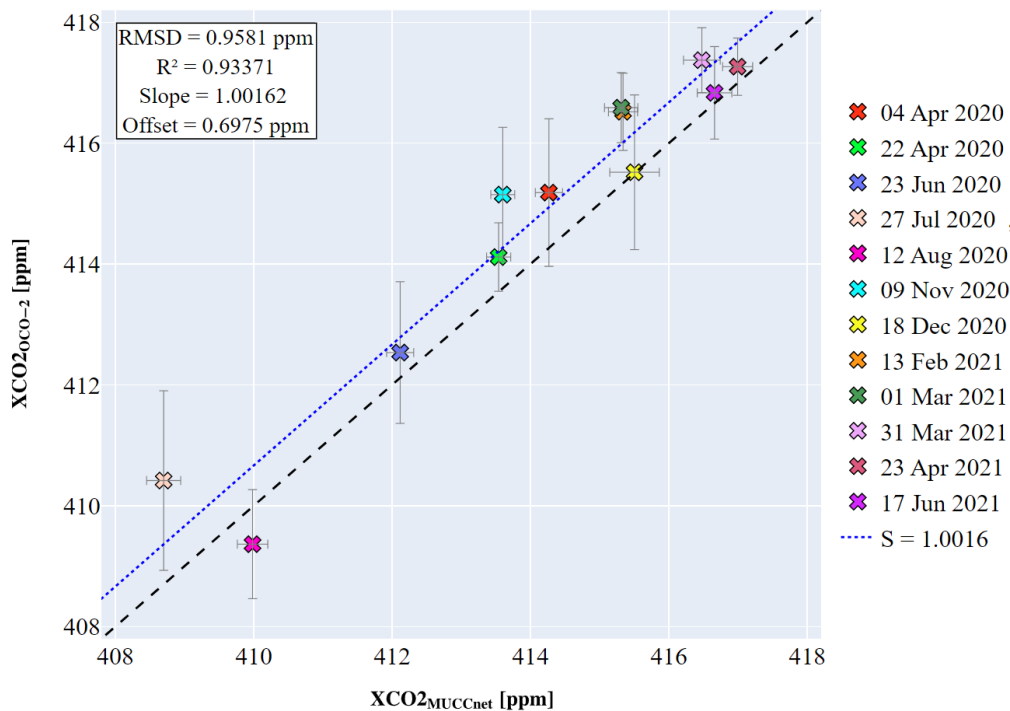
Figure 7. Scatter plot of MUCCnet and OCO-2 X_{CO2} in the comparison time frame. Each overpass is color-coded. The error bars represent the standard deviations of the samples in the corresponding domain.

Figure 8 shows the differences between space-borne and ground-based X_{CO2} retrievals for each individual overpass. Both
235   observing systems capture a similar seasonal behaviour of urban X_{CO2} in Munich in the time period analyzed here. Both OCO-2 and MUCCnet measurements also capture a similar seasonal cycle in X_{CO2}. For eleven out of the twelve overpasses, OCO-2 measured the higher mole fractions, causing an average OCO-2 high bias of 0.7 ppm. Only one overpass (August 12, 2020), OCO-2 captured lower mean X_{CO2} than MUCCnet. On two days a mean offset higher than 1.5 ppm is measured, which is likely caused by sub-optimal measurement conditions. On November 9, 2020 more than 80 % of retrievals are low quality ($qf = 1$)
240   yielding just 816 usable soundings. In the study time, the bias in the satellite data does not show a noticeable temporal drift. The four overpasses in which the space-borne X_{CO2} offset deviates the most from the mean bias took place between July 27, 2020 and December 18, 2020.
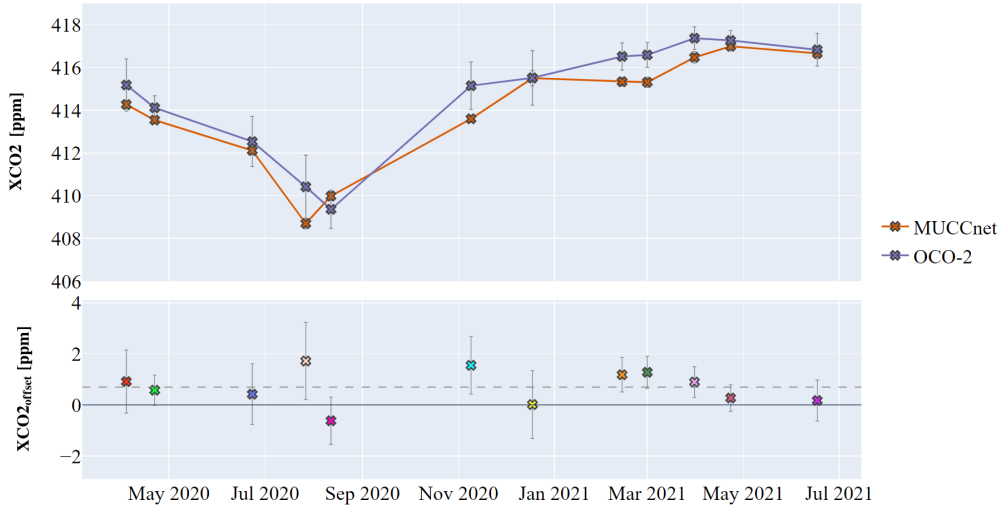
Figure 8. Both observing systems detect the seasonal X_{CO2} variations and a X_{CO2} growth in the study period. The lower panel shows the daily X_{CO2} differences of satellite data and MUCCnet observations. The space-borne observations are biased high by 0.7 ppm.

4.2 By-site validation

245 Dividing the OCO-2 target observations into spatially separated comparison domains allows us to validate the space-borne X_{CO2} in the north (OBE), center (TUM) and west (GRÄ) of Munich. In each domain we consider space-borne soundings that are within a 6 km distance of the collocated MUCCnet instrument. The centre domain usually has the highest amount of space-borne soundings, because the northern and western instruments are closer to the edge of the target area. In contrast to the target comparison in section 4.1 we consider a spatially more constrained subset of OCO-2 soundings. This improves the root mean

250 square differences of OCO-2 and the MUCCnet centre site to $RMSD_{TUM} = 0.82$ ppm. This improvement is caused by more specific collocation, that reduces the effect of averaging over potential spatial X_{CO2} gradients in the OCO-2 target observation. The scatter plots in Fig. 9 show the by-site comparison results for target observations in the study. Similar to the results in the centre domain, for the two remaining MUCCnet sites, we find RMSD values of less than 1 ppm ($RMSD_{GRÄ} = 0.61$ ppm and $RMSD_{OBE} = 0.94$ ppm) when compared to the collocated ground-based measurement sites. Furthermore, all three scatter

255 plots show improved coefficients of determination ($R^2_{TUM} = 0.96$, $R^2_{GRÄ} = 0.97$ and $R^2_{OBE} = 0.96$) when compared to the target validation results in Section 4.1.

We computed a high bias of OCO-2 against the MUCCnet spectrometers in all three comparison domains ranging from $b_{GRÄ} = 0.36$ ppm over $b_{TUM} = 0.59$ ppm to $b_{OBE} = 0.78$ ppm. The differences in the relative location of the collocated OCO-2 soundings in the target field-of-view could impact the results due to changes in the viewing geometry of the space-

260 borne instruments. A larger sample size is required to make a more robust statement. The best fit RMSE is nearly identical
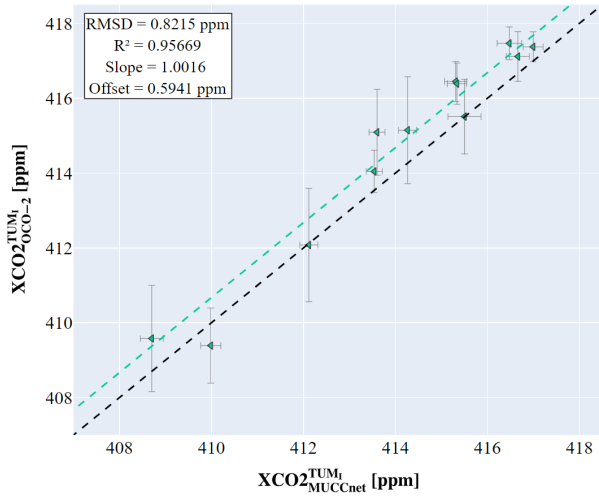
(a) MUCCnet centre X_{CO2} versus collocated OCO-2 X_{CO2} (centre domain)
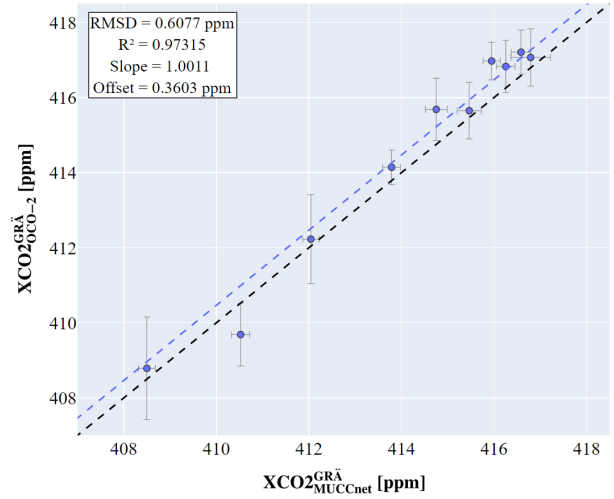
(b) MUCCnet X_{CO2} in Gräfelfing versus collocated OCO-2 X_{CO2} (western domain)
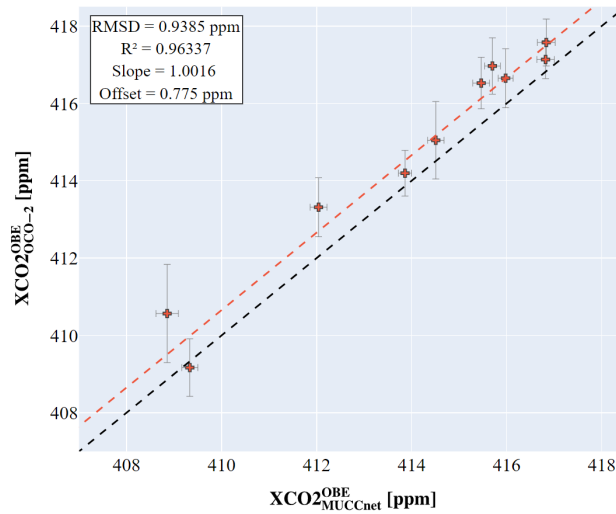
(c) MUCCnet X_{CO2} in Oberschleißheim versus collocated OCO-2 X_{CO2} (northern domain)

Figure 9. By-site comparison results between OCO-2 and MUCCnet. We use the same color coding as in Fig. 5. OCO-2 has the largest bias and RMSD in the northern domain. The error bars represent the standard deviations of the samples in the corresponding domain.

for all three comparison domains ($RMSE_{TUM} = 0.57$ ppm, $RMSE_{GRÄ} = 0.57$ ppm and $RMSE_{OBE} = 0.57$ ppm).. A summary of the linear regression results for target and by-site validation is given in Table 2.

The daily offsets in each domain are depicted in Fig. 10. We assume, measurement uncertainties and the relatively small sample size of eleven overpass days to cause the discrepancies in the computed mean biases of the three collocation domains.

Domain	RMSD (ppm)	R^2	Bias (ppm)	RMSE (ppm)
centre (TUM)	0.822	0.957	0.594	0.57
west (GRÄ)	0.608	0.973	0.360	0.57
north (OBE)	0.939	0.963	0.776	0.57
Target Comparison (Sec. 4.1)	0.958	0.934	0.698	0.66

Table 2. Regression results of collocated X_{CO2} measured by MUCCnet and OCO-2 of by-site and target validation. In all domains OCO-2 is biased high against MUCCnet.
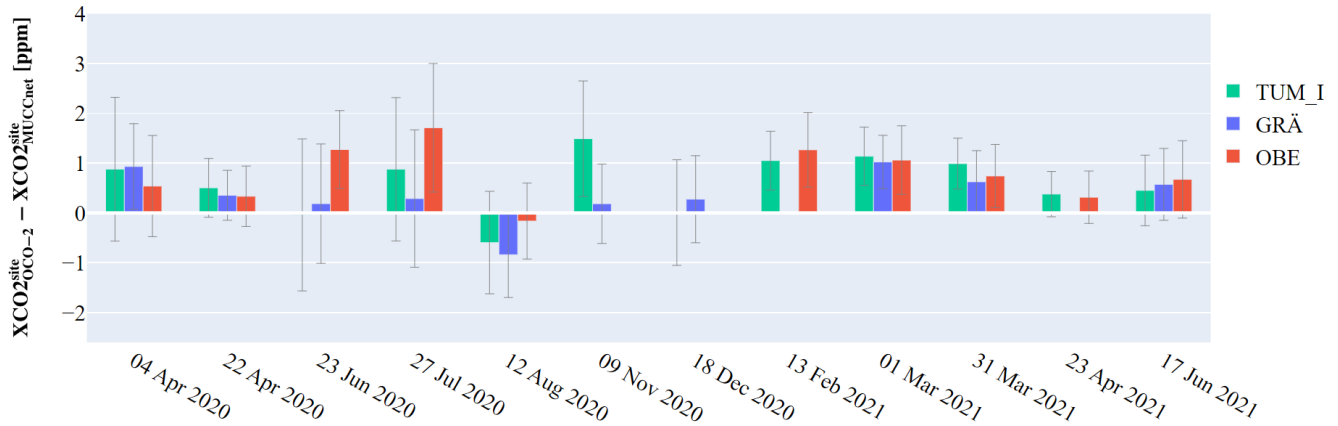
Figure 10. Daily offsets of collocated X_{CO2} captured by OCO-2 and MUCCnet in each comparison domain. During most overpasses the by-site offsets are alike for all comparison domains. However, during some overpasses (eg. Jun 23, Jul 27, Nov 9) we observe a higher level of intra-day variation of the daily by-site offsets, which can impede the detection of urban gradients.

265   OCO-2 retrieves higher CO_2 mole fractions than MUCCnet in all three domains, during each overpass except for August 12, 2020. For most overpasses the by-site offsets are consistent in each of the three collocation areas. The largest discrepancies in daily offsets in the three domains could be observed on overpass days with a smaller than average number of good quality soundings (e.g. November 9, 2020 and July 27, 2020). Target observations with a high number of good quality soundings in general have had smaller differences in daily by-site X_{CO2} offsets.

270

   Overall, we discover an improvement of RMSD and a higher correlation R^2 in the by-site validation when compared to the target validation due to the smaller collocation radius. OCO-2 is well capable of detecting X_{CO2} in the three domains in the centre, west and north of Munich. However, small differences in averaged bias are present in the three collocation areas.

4.3 Assessment of urban X_{CO2} gradients measured from space

275 The adjusted collocation procedure also allows us to assess the space-borne CO_2 gradients in the OCO-2 target observations. This is the first time gradients within one OCO-2 target observations are evaluated against measurements of multiple ground-based measurements sites. We contrast the space-borne $\Delta XCO2_{OCO-2}$ against the X_{CO2} differences measured by the collocated MUCCnet spectrometers during the overpass (see Fig. 11). This simple approach allows us to see how spatial X_{CO2} gradients in the target observations compare to the X_{CO2} differences captured by MUCCnet. We compute three sets of gradients

280 (north-west, north-centre and west-centre), for each overpass, where a sufficient amount of data is available.
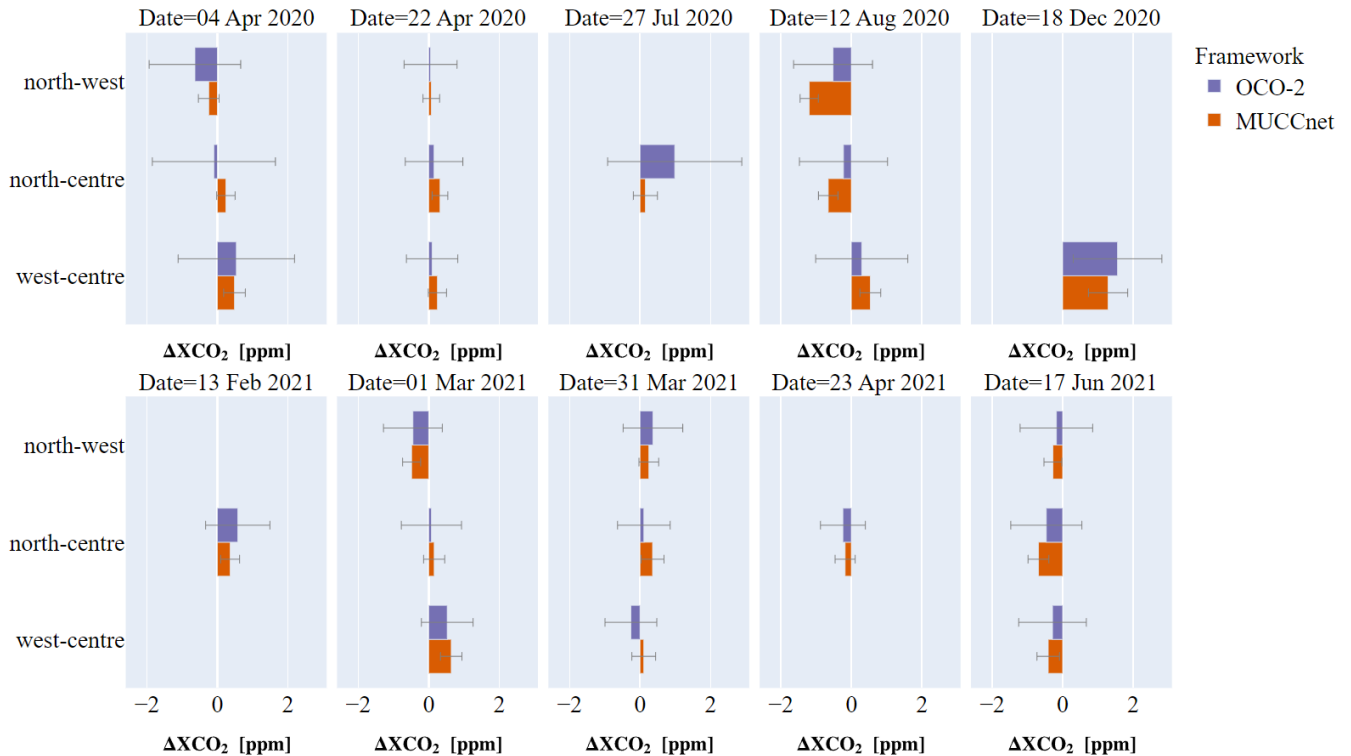
Figure 11. X_{CO2} gradients in Munich on overpass days. Blue bars represent the gradients present in the OCO-2 target observations. Orange bars denote X_{CO2} gradients captured by MUCCnet. On most days, OCO-2 sees elevated X_{CO2} in the same region as the ground-based MUCCnet instruments. Error bars are computed using the combined standard deviations of the X_{CO2} retrievals used for computing each gradient. (see Eq. 6).

X_{CO2} enhancements in Munich are usually in the range from 0.1 to 1.0 ppm during the overpasses featured in this study. This coincides with results of previous urban gradient assessments in Munich published in Dietrich et al. (2021). On average, the MUCCnet instruments measured site to site enhancements of 0.42 ppm. These rather low gradients allow us to test the lower

 detection limits of OCO-2 for resolving small scale gradients.

(a) All three subsets of X_{CO2} gradients show a strong correlation.

(b) North-west X_{CO2} gradients.

(c) West-centre X_{CO2} gradients

(d) North-centre X_{CO2} gradients
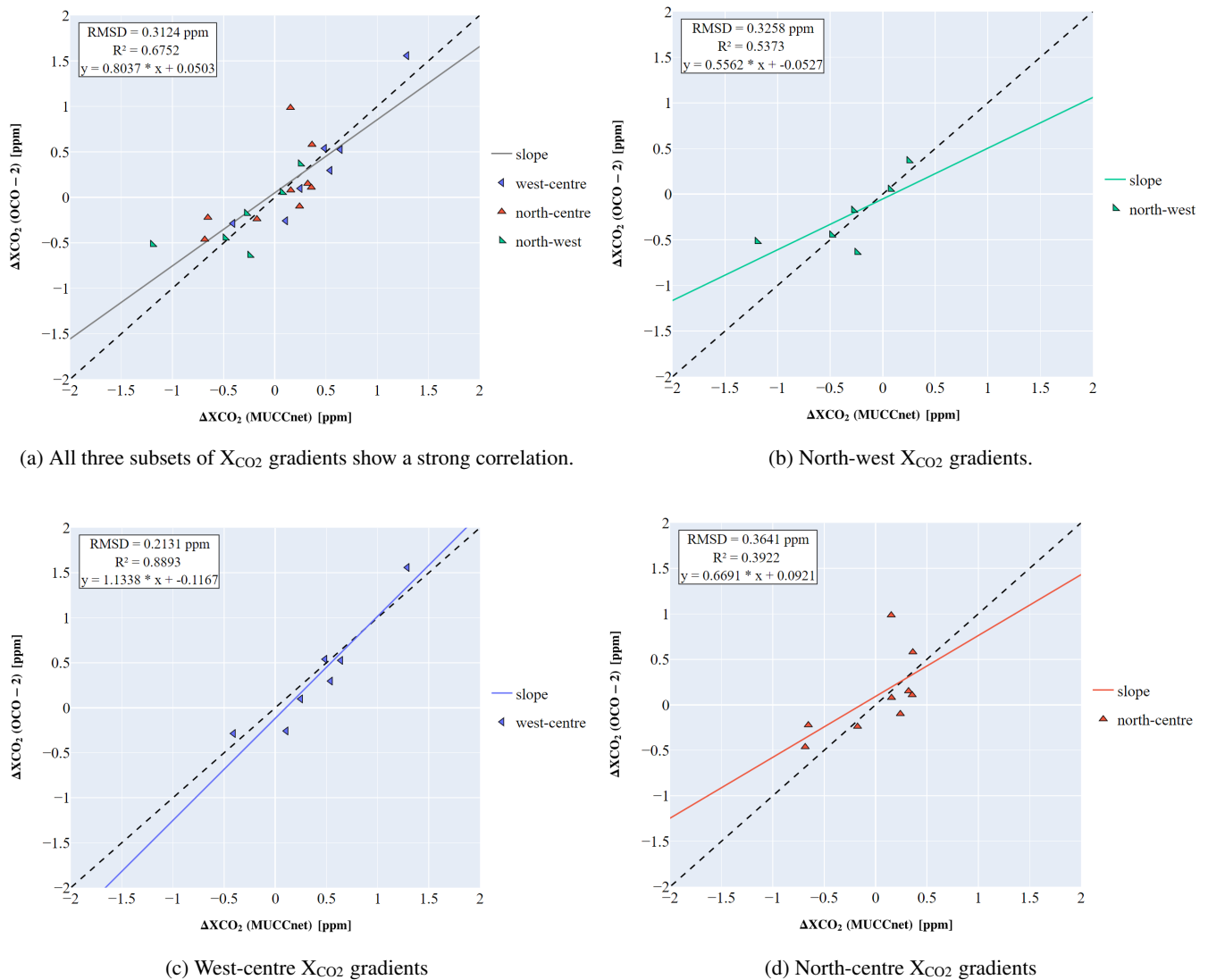
Figure 12. Linear regression results of space-borne and ground-based X_{CO2} differences. Depending on the subset of gradients we observe moderate to very strong correlation between ground-based and space-borne gradients. These differences in agreement are caused by single outliers, which impact the regression results due to the small sample size and low absolute gradients in Munich.

Considering the rather small X_{CO2} gradients in Munich, OCO-2 detects the elevated X_{CO2} in the same domain as MUCCnet for 20 of the 22 computed gradients and therefore qualitatively determines the area of enhanced X_{CO2} correctly in 91 % of cases. Furthermore, for 68 % (15/22) of the computed gradients, OCO-2 is within a margin of error of just 0.25 ppm when

290   compared to the more precise MUCCnet measurements. For the entire set of gradients OCO-2 achieved an $RMSD$ of 0.31 ppm and a linear correlation with a strong correlation of $R^2 = 0.68$ between OCO-2 and the MUCCnet measurements.

In particular, for west-centre gradients (between TUM and Gräfelfing) space-borne and ground-based X_{CO2} gradients are highly correlated ($R^2_{west-centre} = 0.89$) with a $RMSD = 0.21$ ppm. The space-borne north-west and north-centre gradients have higher RMSDs and are moderately correlated ($R^2_{north-west} = 0.39$, $R^2_{north-centre} = 0.54$) to the X_{CO2} gradients mea-

295   sured by the MUCCnet spectrometers. For the north-west and north-centre X_{CO2} differences the RMSD is 0.33 ppm and 0.36 ppm, respectively. Due to the low sample size, the space-borne X_{CO2} gradients captured on July 27, 2020 and August 12, 2020 strongly impact the regression results for the north-west and north-centre subsets. Here, north-west and north-centre X_{CO2} differences, captured by OCO-2, are off more than 0.5 ppm. During both overpasses, we observe a higher X_{CO2} offset in the northern domain than in the other two domains (see Fig. 10). Due to the low absolute X_{CO2} gradients that are captured during

300   our study and the relatively low sample size, single outlier overpasses have a strong impact on the regression results. Conse-quently, if we remove both outlier days, July 27 and August 12, we achieve an overall improved RMSD and strong correlation for all subsets of gradients. These improved results are shown in Fig. A2 in the Appendix A2. We expect more robust and definitive results for a larger sample size. It's important to be aware of the measurement context. Generally, we see a better agreement in gradients for days with a high yield of good quality soundings and good measurement conditions.

305

    There is no tendency towards one observational method showing systematically higher or lower gradients than the other. On some days, MUCCnet measured greater X_{CO2} enhancements in the suburban sites when compared to the OCO-2 observations like it is the case on April 22, 2020 and March 1, 2021. During the overpasses on December 18, 2020 and February 2, 2021, OCO-2 detected slightly higher X_{CO2} gradients than MUCCnet.

310

    The overall strong correlation shows that OCO-2 is capable of detecting similar mean X_{CO2} differences as MUCCnet. Even though the spread of the space-borne measurements in each domain is sometimes larger than the gradients itself, the X_{CO2} means in each domain are robust enough to capture the small urban gradients between the domains from space. These results show that OCO-2 target observations capture valuable information about the spatial distribution of X_{CO2} within one OCO-2 tar-

315   get field-of-view. If the measurement conditions are good, OCO-2 target mode can successfully capture urban X_{CO2} gradients in Munich. It leads to the conclusion that OCO-2 is capable of detecting intra-urban X_{CO2} fluxes and enhancements, caused by anthropogenic activities on a sub-city scale. Hence, OCO-2 target observations could find more use in assessing area sources of CO_2 from space.

320 **4.4 X_{CO2} enhancements on December 18, 2020**

December 18, 2020 was the only overpass on which ground-based centre-west X_{CO2} enhancements are greater than 1 ppm. During the one hour overpass collocation time, CO_2 retrievals in Gräfelfing ($XCO2_{MUCCnet} = 416.8 \pm 0.43$) exceeded the mean X_{CO2} in Munichs city center by $\Delta XCO2_{MUCCnet} = 1.3$ ppm. The center spectrometer measured $XCO2_{MUCCnet} =$

415.5±0.36 ppm during the overpass. On this day the collocated OCO-2 is in good agreement with its ground based counterpart
(see Fig. 13). Hence, OCO-2 observes similarly large enhancements of $\Delta XCO2_{OCO-2} = 1.55$ ppm in the west of Munich.
X_{CO2} enhancements between an upwind and a downwind measurement site is caused by natural and anthropogenic emissions
and the subsequent atmospheric transport (Chen et al., 2016). We use ERA5 wind data within ±2 h of the overpass time to
evaluate which of the measurement sites are positioned downwind and upwind during the overpass. On December 18, 2020
the mostly east and east-south-east winds with relatively low wind speeds of less than 1.91 m/s are reported. Thus, convective
transport of anthropogenic CO_2 emissions in the urban centre of Munich towards the west causes enhanced X_{CO2} in the western
comparison domain. Both, ground-based and satellite measurements capture similar X_{CO2} enhancements, that are higher than
usual.
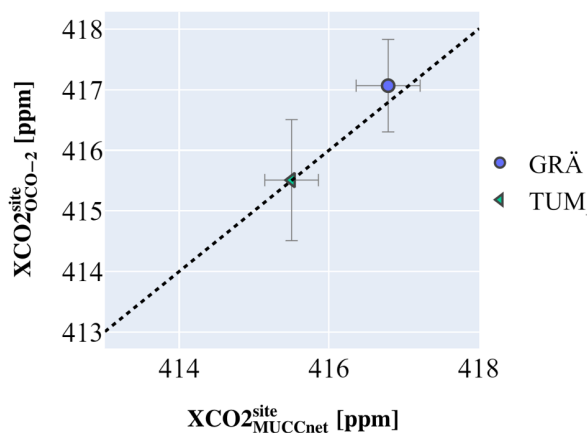
Figure 13. X_{CO2} captured by OCO-2 and MUCCnet
on December 18, 2020
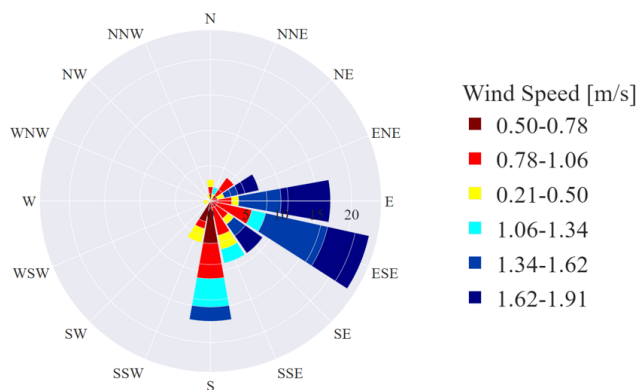
Figure 14. ERA5 wind rose ±2 h of overpass time.

The spatial distribution of X_{CO2} in Munich is shown in Fig. 15a. The lowest X_{CO2} is measured in the south-east and north of
Munich with increasingly higher mole fractions in the centre. The highest X_{CO2} is captured right at the western edge of the tar-
get field-of-view close to the MUCCnet site in Gräfelfing. Here, single soundings reach peak mole fractions of up to 418.6 ppm.

A qualitative comparisons of the OCO-2 target overpass to the satellite retrievals shows, that OCO-2 and the WRF-GHG
produce a similar spatial distribution of urban X_{CO2} during the overpass. The plots in Fig. 15 show both the X_{CO2} captured by
OCO-2 (left) and the X_{CO2} generated via the WRF model (right). The gridded WRF results have an overall higher mean X_{CO2} of
$XCO2_{WRF} = 417.32 \pm 0.21$ ppm while the satellite retrieves $XCO2_{OCO2} = 415.15 \pm 1.3$ ppm. Nonetheless, both approaches
have the highest CO_2 mole fractions in the west. A plume-like shape originating in the centre of Munich extends westwards.
OCO-2 captures a broader spread of X_{CO2} in contrast to the more distinct plume shape generated by the WRF-GHG model.
The lowest mole fractions are modelled and retrieved in the south-east and north-east. The spread of mole fractions, that is
captured by OCO-2, is considerably higher than the outputs of the WRF-GHG simulation. We qualitatively compare the X_{CO2}
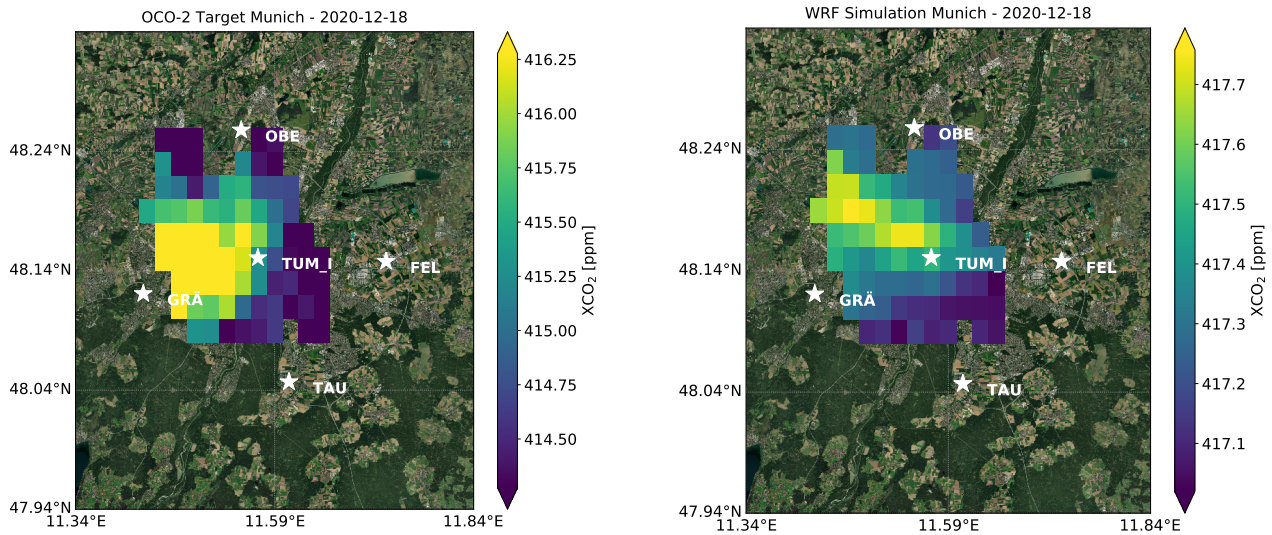
(a) X$_{CO2}$ target observation taken on
December 18, 2020 - 12:02 UTC

(b) Gridded XCO2$_{\mathrm{WRF}}$ at 12:00 UTC - 2 minutes before the OCO-2
overpass.

Figure 15. Gridded WRF-GHG outputs and OCO-2 target observation for December 18th, 2020. Enhanced X$_{CO2}$ is predominantly captured in the centre west of Munich.

345   differences captured by OCO-2 and MUCCnet to the X$_{CO2}$ enhancements of the WRF-GHG simulation. A mismatch in model wind speed and direction causes the area of maximum X$_{CO2}$ enhancements to be shifted to the north in the model data (see Fig. 15). The enhancements measured by the satellite and MUCCnet ($\Delta \mathrm{XCO2}^{\mathrm{west}}_{\mathrm{OCO}-2} = 1.55$ ppm and $\Delta \mathrm{XCO2}^{\mathrm{west}}_{\mathrm{MUCCnet}} = 1.23$ ppm) are higher than the X$_{CO2}$ gradients in the WRF-GHG simulation. The plume of the model originating south-east shows enhancements of up to around 0.5 ppm in the centre of the plume (compare Fig. 15b). The satellite observations resemble the

350   precise retrievals, measured by the MUCCnet instruments, better than the WRF-GHG model. We assume this underestimation of X$_{CO2}$ gradients to be caused by both, uncertainties in the annual emission inventory as well as transport uncertainties. Furthermore, the X$_{CO2}$ in the target observation is notably higher than on other days, indicating unusually high emissions in Munich on December 18, 2020, which can't be replicated by a yearly-averaged bottom-up emission inventory, while the spatial distribution is reproduced rather accurately. We recognize the potential of space-borne X$_{CO2}$ retrievals in reducing the

355   mentioned uncertainties in the model transport and emission inventories. These results suggest that for high gradients and cloud free measurement conditions, OCO-2 target observations can be utilized for an accurate assessment of urban X$_{CO2}$ and its spatial distribution.

5   Conclusion

Comparisons between OCO-2 target measurements over Munich, Germany and ground-based measurements performed by
360   MUCCnet's reference instrument agree well for the analyzed time period with a RMSD value of 0.96 ppm. On all days, OCO-

2 appears to be biased high with a mean offset of 0.7 ppm. This bias is similar to comparisons between OCO-2 and the TCCON site in Karlsruhe. In the by-site comparison we find a improved correlation and reduced RMSDs in all three spatially separated comparison domains (centre, west, north), due to the smaller collocation area, which reduces the impact of potential spatial X_{CO2} gradients in the target field on the validation results.

365   For the first time, sub-city scale X_{CO2} variations in the OCO-2 target measurements were cross compared against collocated ground-based X_{CO2} gradients captured by multiple MUCCnet sites. Due to the relatively small spatial X_{CO2} differences of mostly below 0.5 ppm in Munich we were able to test the lower detection limits for sub-city scale gradients. Even though, OCO-2's proclaimed precision of 1 ppm is larger than most gradients we captured during our study, we found moderate to strong aggreement between MUCCnet and OCO-2 X_{CO2} gradients and root mean square values of 0.21 to 0.36 ppm. For more

370 than 90% of the captured gradients, OCO-2 was able to detect the correct direction of the X_{CO2} gradients. The overall low X_{CO2} differences in Munich and the limited number of overpasses featured in this study make it hard to draw more definitive conclusions for now. We expect urban monitoring networks like MUCCnet to play a crucial role in validating space-borne X_{CO2} gradients of wide swath CO_2 monitoring missions in the future. It will be interesting to see how OCO-2 and OCO-3 will perform against similar setups in megacities and larger industrial areas.

375   Finally, the qualitative comparisons to WRF-model data on December 18, 2020 reveal a matching spatial distribution of target and model X_{CO2}. Emissions in the city centre are transported westwards and cause enhanced X_{CO2} close to the western MUCCnet site in Gräfelfing. This points to OCO-2's potential of locating highly potent emission sources and providing valuable insight for future model development.

    All things considered, we see the potential of OCO-2 to provide vital information about urban gradients in cities, agglomer-

380 ated areas and other potent CO_2 emitters around the globe that further improves the understanding of the relevance of anthropogenic urban emissions for our climate. We hope, the measurement of urban X_{CO2} gradients from space will be a powerful tool for evaluating urban anthropogenic emission, globally. Further comparisons of OCO-2 target observations to ground-based monitoring networks are beneficial to better understand OCO-2's capability of assessing point and area sources from space.

385 *Acknowledgements.* We thank Friedrich Klappenbach for his help on setting up the PROFFAST retrieval locally for the five EM27/SUN instruments, Franziska Dobler for helping with the WRF-GHG data processing. Special thanks to our colleagues at the Jet Propulsion Laboratory (JPL) and their OCO-2 team for regularly targeting Munich as well as always being supportive and providing researchers with high quality data and support. We also want to thank our reviewers for their valuable inputs, that helped us to revise our manuscript.

Author contributions. MR wrote the manuscript in cooperation with JC. MK, XZ, FD, GO and FH edited the manuscript. FD and JC

390 set up the ground-based remote sensing network in Munich (MUCCnet), that provides the EM27/SUN datasets. MK and GO guided the research with their expertise on the OCO ACOSv10 datasets. MK provided up to date TCCON comparison results. XZ set up the WRF-model framework in Munich and provided us with the WRF-GHG datasets. MM set up and automated the PROFFAST retrieval for all five

measurement sites in Munich. MR conducted collocation and validation data processing and visualization of our results. FH provided us valuable information about the PROFFAST retrieval and post-correction. JC, MK and FD supervised the the research.

Competing interests. We declare no conflicts of interest with this research.

Code and data availability. All OCO-2 data files are available at the GES DISC data centre (GES DISC, 2021). All PROFFAST retrieval files and WRF-GHG outputs are stored locally on the ESM cloud server and are available at request. Plots are generated using the python plotly library.

A1   Appendix I

400   Figure A1 shows the daily mean X_{CO2} measured by OCO-2 in each comparison domain versus the collocated MUCCnet instrument. In target observations taken on June 23rd, and July 27th, 2020 strong site-to-site X_{CO2} differences are visible in the OCO-2 data while MUCCnet observes little to none X_{CO2} differences between its sites. On August 12th and November 9th, the opposite is true and MUCCnet captures higher X_{CO2} enhancements than OCO-2.
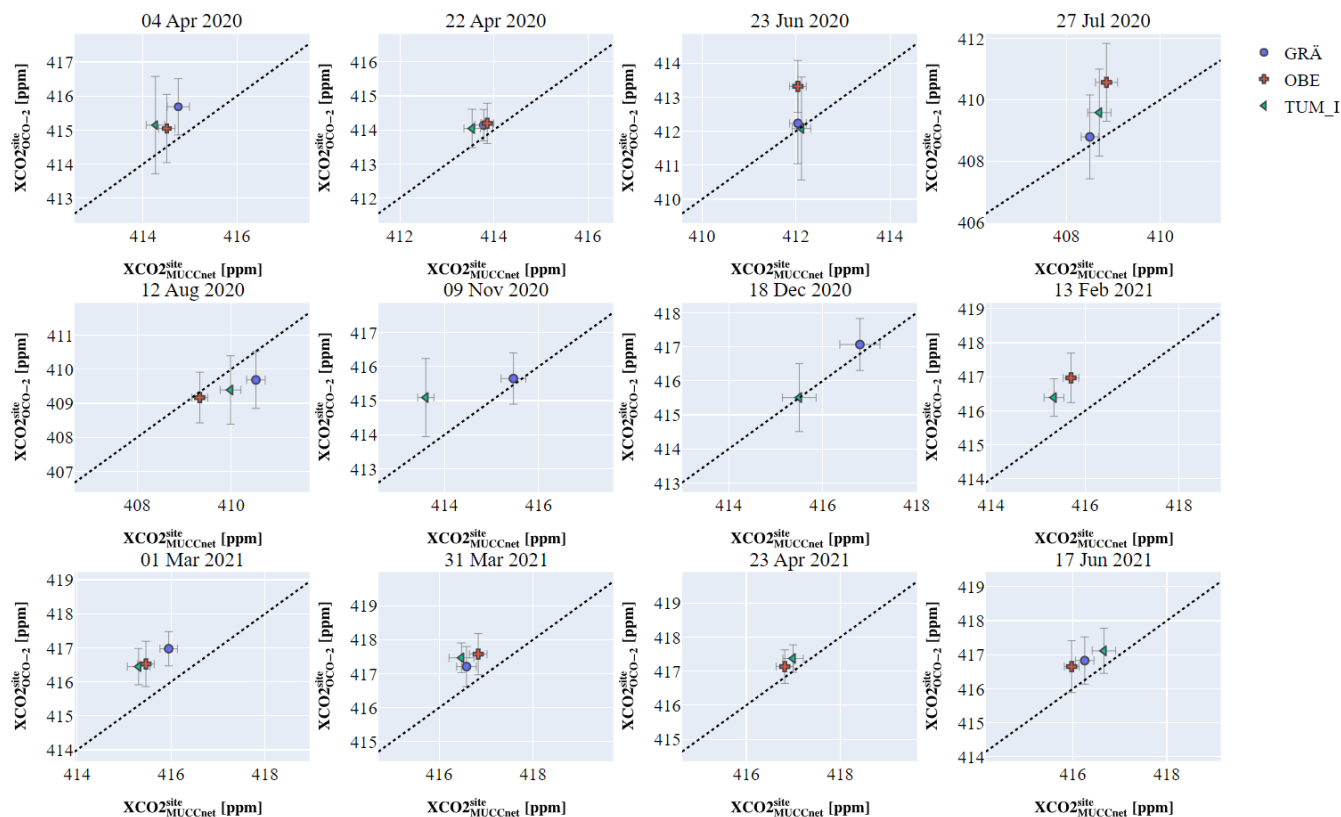
Figure A1. Daily X_{CO2} by-site comparison results.

A2 Appendix II
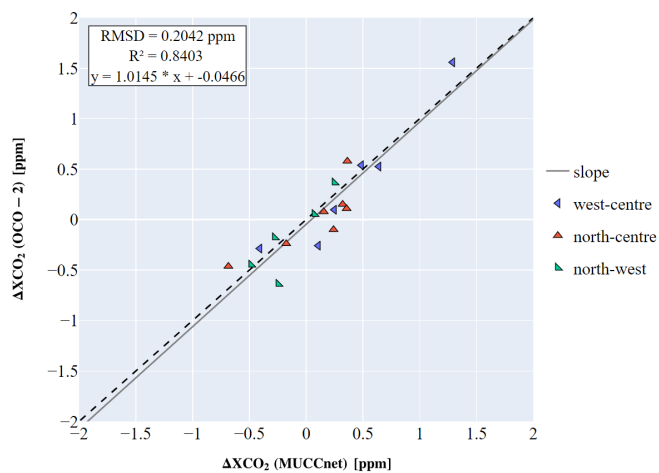
(a) All three subsets of X_{CO2} gradients show a strong correlation.
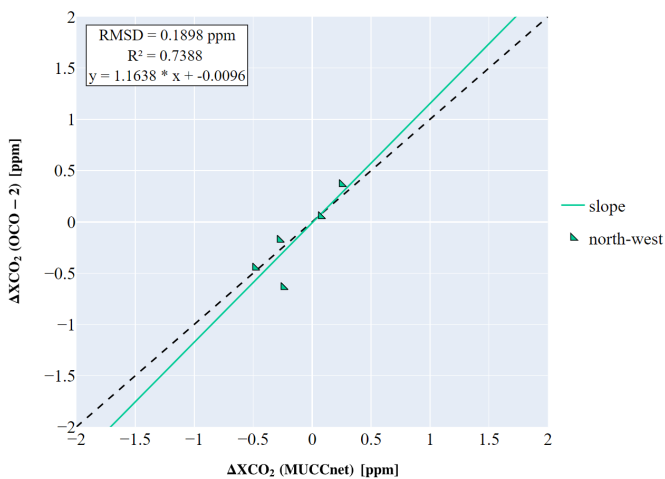
(b) North-west X_{CO2} gradients.
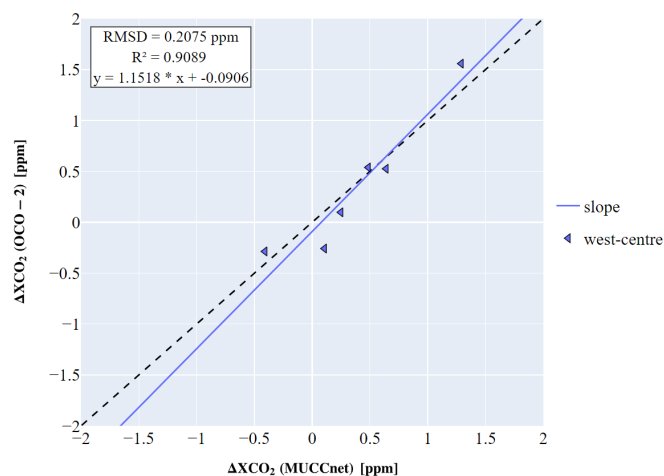
(c) West-centre X_{CO2} gradients
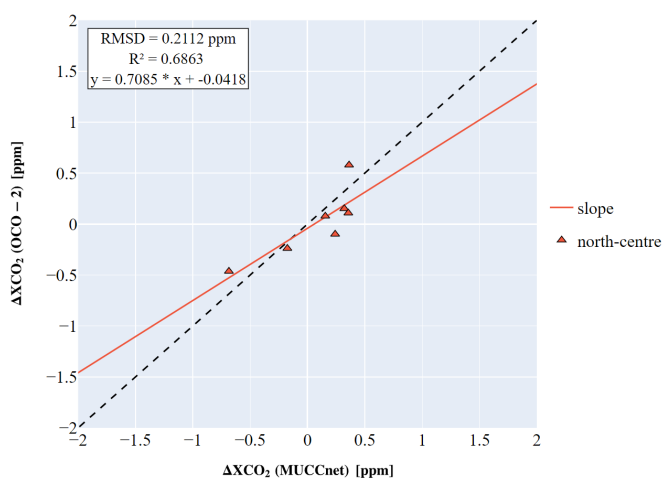
(d) North-centre X_{CO2} gradients

Figure A2. Linear regression results of space-borne and ground-based X_{CO2} enhancements when gradients captured on Aug 18, 2020 and June 27, 2020 are removed from the set. When removing overpasses with a high difference in daily by-site offsets, which impedes the correct detection of urban gradients, we obtain a strong to very strong correlation between OCO-2 and MUCCnet gradients.

References

Alberti, C., Hase, F., Frey, M., Dubravica, D., Blumenstock, T., Dehn, A., Castracane, P., Surawicz, G., Harig, R., Baier, B. C., Bès, C., Bi, J., Boesch, H., Butz, A., Cai, Z., Chen, J., Crowell, S. M., Deutscher, N. M., Ene, D., Franklin, J. E., García, O., Griffith, D., Grouiez, B., Grutter, M., Hamdouni, A., Houweling, S., Humpage, N., Jacobs, N., Jeong, S., Joly, L., Jones, N. B., Jouglet, D., Kivi, R., Kleinschek, R., Lopez, M., Medeiros, D. J., Morino, I., Mostafavipak, N., Müller, A., Ohyama, H., Palmer, P. I., Pathakoti, M., Pollard, D. F., Raffalski, U., Ramonet, M., Ramsay, R., Sha, M. K., Shiomi, K., Simpson, W., Stremme, W., Sun, Y., Tanimoto, H., Té, Y., Tsidu, G. M., Velazco, V. A., Vogel, F., Watanabe, M., Wei, C., Wunch, D., Yamasoe, M., Zhang, L., and Orphal, J.: Improved calibration procedures for the EM27/SUN spectrometers of the COllaborative Carbon Column Observing Network (COCCON), Atmospheric Measurement Techniques, 15, 2433–2463, https://doi.org/10.5194/amt-15-2433-2022, 2022.

Beck, V., Koch, T., Kretschmer, R., Marshall, J., Ahmadov, R., Gerbig, C., Pillai, D., and Heimann, M.: The WRF Greenhouse Gas Model (WRF-GHG) Technical Report, https://www.bgc-jena.mpg.de/bgc-systems/pmwiki2/uploads/Download/Wrf-ghg/WRF-GHG_Techn_Report.pdf, 2011.

Chen, J., Viatte, C., Hedelius, J. K., Jones, T., Franklin, J. E., Parker, H., Gottlieb, E. W., Wennberg, P. O., Dubey, M. K., and Wofsy, S. C.: Differential Column Measurements Using Compact Solar-Tracking Spectrometers, Atmospheric Chemistry and Physics, 16, 8479–8498, https://doi.org/10.5194/acp-16-8479-2016, 2016.

Chen, J., Dietrich, F., Forstmaier, A., Bettinelli, J., Maazallahi, H., Röckmann, T., Winkler, D., Zhao, X., Makowski, M., Veen, C. V. D., Wildmann, N., Jones, T., Ament, F., and Lange, I.: Multi-scale measurements combined with inverse modeling for assessing methane emissions of Hamburg, 2022.

Crisp, D.: Measuring atmospheric carbon dioxide from space: The GOSAT and OCO-2 missions, Optics InfoBase Conference Papers, 2, https://doi.org/10.1364/e2.2011.ewc6, jet Propulsion Laboratory/California Institute of Technology,, 2011.

Dietrich, F., Chen, J., Voggenreiter, B., Aigner, P., Nachtigall, N., and Reger, B.: MUCCnet : Munich Urban Carbon Column network, pp. 1111–1126, Technische Universität München, 2021.

Dubravica, D. and Hase, F.: Technical note on XCO2 bias in current PROFFAST distribution (10.08.2021), p. 1, Karlsruhe Institute of Technology, 2021.

Frey, M. and Gisi, M.: Calibration of the EM27 / SUN Instruments, https://www.imk-asf.kit.edu/downloads/Coccon/2021-04-30_Instrument-Calibration.pdf, 2021.

Frey, M., Hase, F., Blumenstock, T., Groß, J., Kiel, M., Mengistu Tsidu, G., Schäfer, K., Sha, M. K., and Orphal, J.: Calibration and instrumental line shape characterization of a set of portable FTIR spectrometers for detecting greenhouse gas emissions, Atmospheric Measurement Techniques, 8, 3047–3057, https://doi.org/10.5194/amt-8-3047-2015, 2015.

Frey, M., Sha, M. K., Hase, F., Kiel, M., Blumenstock, T., Harig, R., Surawicz, G., Deutscher, N. M., Shiomi, K., Franklin, J. E., Bösch, H., Chen, J., Grutter, M., Ohyama, H., Sun, Y., Butz, A., Mengistu Tsidu, G., Ene, D., Wunch, D., Cao, Z., Garcia, O., Ramonet, M., Vogel, F., and Orphal, J.: Building the COllaborative Carbon Column Observing Network (COCCON): Long-term stability and ensemble performance of the EM27/SUN Fourier transform spectrometer, Atmospheric Measurement Techniques, 12, 1513–1530, https://doi.org/10.5194/amt-12-1513-2019, 2019.

GES DISC: OCO-2 Level 2 bias-corrected XCO2 and other select fields from the full-physics retrieval aggregated as daily files, Retrospective processing V10r, https://disc.gsfc.nasa.gov/datasets/, accessed: 2021-11-29, 2021.

Gisi, M., Hase, F., Dohe, S., Blumenstock, T., Simon, A., and Keens, A.: XCO 2-measurements with a tabletop FTS using solar absorption spectroscopy, Atmospheric Measurement Techniques, 5, 2969–2980, 2012.

Gurney, K. R., Romero-Lankao, P., Seto, K. C., Hutyra, L. R., Duren, R., Kennedy, C., Grimm, N. B., Ehleringer, J. R., Marcotullio, P., Hughes, S., Pincetl, S., Chester, M. V., Runfola, D. M., Feddema, J. J., and Sperling, J.: Climate change: Track urban emissions on a human scale, Nature, 525, 179–181, https://doi.org/10.1038/525179a, 2015.

Hase, F., Hannigan, J., Coffey, M., Goldman, A., Höpfner, M., Jones, N., Rinsland, C., and Wood, S.: Intercomparison of retrieval codes used for the analysis of high-resolution, ground-based FTIR measurements, Journal of Quantitative Spectroscopy and Radiative Transfer, 87, 25–52, https://doi.org/10.1016/j.jqsrt.2003.12.008, 2004.

Hase, F., Frey, M., Blumenstock, T., Groß, J., Kiel, M., Kohlhepp, R., Mengistu Tsidu, G., Schäfer, K., Sha, M., and Orphal, J.: Application of portable FTIR spectrometers for detecting greenhouse gas emissions of the major city Berlin, Atmospheric Measurement Techniques, 8, 3059–3068, 2015.

Heinle, L. and Chen, J.: Automated enclosure and protection system for compact solar-tracking spectrometers, Atmospheric Measurement Techniques, 11, 2173–2185, https://doi.org/10.5194/amt-11-2173-2018, 2018.

Jacobs, N., Simpson, W. R., Wunch, D., O'Dell, C. W., Osterman, G. B., Hase, F., Blumenstock, T., Tu, Q., Frey, M., Dubey, M. K., Parker, H. A., Kivi, R., and Heikkinen, P.: Quality controls, bias, and seasonality of CO2 columns in the boreal forest with Orbiting Carbon Observatory-2, Total Carbon Column Observing Network, and EM27/SUN measurements, Atmospheric Measurement Techniques, 13, 5033–5063, https://doi.org/10.5194/amt-13-5033-2020, 2020.

Jones, T. S., Franklin, J. E., Chen, J., Dietrich, F., Hajny, K. D., Paetzold, J. C., Wenzel, A., Gately, C., Gottlieb, E., Parker, H., Dubey, M., Hase, F., Shepson, P. B., Mielke, L. H., and Wofsy, S. C.: Assessing urban methane emissions using column-observing portable Fourier transform infrared (FTIR) spectrometers and a novel Bayesian inversion framework, Atmospheric Chemistry and Physics, 21, 13 131–13 147, https://doi.org/10.5194/acp-21-13131-2021, 2021.

Kiel, M.: OCO-2 Science Team Telecon: A six year record of OCO-2 XCO2 measurements, 2021.

Kiel, M., O'Dell, C. W., Fisher, B., Eldering, A., Nassar, R., MacDonald, C. G., and Wennberg, P. O.: How bias correction goes wrong: measurement of XCO2 affected by erroneous surface pressure estimates, Atmospheric Measurement Techniques, 12, 2241–2259, https://doi.org/10.5194/amt-12-2241-2019, 2019.

Kiel, M., Eldering, A., Roten, D. D., Lin, J. C., Feng, S., Lei, R., Lauvaux, T., Oda, T., Roehl, C. M., Blavier, J. F., and Iraci, L. T.: Urban-focused satellite CO2 observations from the Orbiting Carbon Observatory-3: A first look at the Los Angeles megacity, Remote Sensing of Environment, 258, https://doi.org/10.1016/j.rse.2021.112314, 2021.

Luther, A., Kleinschek, R., Scheidweiler, L., Defratyka, S., Stanisavljevic, M., Forstmaier, A., Dandocsi, A., Wolff, S., Dubravica, D., Wildmann, N., Kostinek, J., Jöckel, P., Nickl, A.-L., Klausner, T., Hase, F., Frey, M., Chen, J., Dietrich, F., Nęcki, J., Swolkień, J., Fix, A., Roiger, A., and Butz, A.: Quantifying CH$_4$ emissions from hard coal mines using mobile sun-viewing Fourier transform spectrometry, Atmospheric Measurement Techniques, 12, 5217–5230, https://doi.org/10.5194/amt-12-5217-2019, 2019.

Luther, A., Kostinek, J., Kleinschek, R., Defratyka, S., Stanisavljevic, M., Forstmaier, A., Dandocsi, A., Scheidweiler, L., Dubravica, D., Wildmann, N., Hase, F., Frey, M. M., Chen, J., Dietrich, F., Necki, J., Swolkien, J., Knote, C., Vardag, S. N., Roiger, A., and Butz, A.: Observational constraints on methane emissions from Polish coal mines using a ground-based remote sensing network, Atmospheric Chemistry and Physics Discussions, 2021, 1–27, https://doi.org/10.5194/acp-2021-978, 2021.

Makarova, M. V., Alberti, C., Ionov, D. V., Hase, F., Foka, S. C., Blumenstock, T., Warneke, T., Virolainen, Y. A., Kostsov, V. S., Frey, M., Poberovskii, A. V., Timofeyev, Y. M., Paramonova, N. N., Volkova, K. A., Zaitsev, N. A., Biryukov, E. Y., Osipov, S. I., Makarov,

B. K., Polyakov, A. V., Ivakhov, V. M., Imhasin, H. K., and Mikhailov, E. F.: Emission Monitoring Mobile Experiment (EMME):
480   an overview and first results of the St. Petersburg megacity campaign 2019, Atmospheric Measurement Techniques, 14, 1047–1073,
         https://doi.org/10.5194/amt-14-1047-2021, 2021.

Montzka, S.: The NOAA Annual Greenhous Gas Index (AGGI), https://gml.noaa.gov/aggi/aggi.html, 2021.

Nguyen, H., Osterman, G., Wunch, D., O'Dell, C., Mandrake, L., Wennberg, P., Fisher, B., and Castano, R.: A method for colocating
         satellite XCO2 data to ground-based data and its application to ACOS-GOSAT and TCCON, Atmospheric Measurement Techniques, 7,
485   2631–2644, https://doi.org/10.5194/amt-7-2631-2014, 2014.

O'Dell, C. W., Connor, B., Bösch, H., O'Brien, D., Frankenberg, C., Castano, R., Christi, M., Eldering, D., Fisher, B., Gunson, M., McDuffie,
         J., Miller, C. E., Natraj, V., Oyafuso, F., Polonsky, I., Smyth, M., Taylor, T., Toon, G. C., Wennberg, P. O., and Wunch, D.: The ACOS CO_2
         retrieval algorithm – Part 1: Description and validation against synthetic observations, Atmospheric Measurement Techniques, 5, 99–121,
         https://doi.org/10.5194/amt-5-99-2012, 2012.

490 O'Dell, C. W., Eldering, A., Wennberg, P. O., Crisp, D., Gunson, M. R., Fisher, B., Frankenberg, C., Kiel, M., Lindqvist, H., Mandrake, L.,
         Merrelli, A., Natraj, V., Nelson, R. R., Osterman, G. B., Payne, V. H., Taylor, T. E., Wunch, D., Drouin, B. J., Oyafuso, F., Chang, A.,
         McDuffie, J., Smyth, M., Baker, D. F., Basu, S., Chevallier, F., Crowell, S. M. R., Feng, L., Palmer, P. I., Dubey, M., García, O. E., Griffith,
         D. W. T., Hase, F., Iraci, L. T., Kivi, R., Morino, I., Notholt, J., Ohyama, H., Petri, C., Roehl, C. M., Sha, M. K., Strong, K., Sussmann,
         R., Te, Y., Uchino, O., and Velazco, V. A.: Improved retrievals of carbon dioxide from Orbiting Carbon Observatory-2 with the version 8
495   ACOS algorithm, Atmospheric Measurement Techniques, 11, 6539–6576, https://doi.org/10.5194/amt-11-6539-2018, 2018.

Osterman, G., ODell, C., Eldering, A., Fisher, B., Crisp, D., Cheng, C., Frankenberg, C., Lambert, A., Gunson, M. R., Mandrake, L., and
         Wunch, D.: Orbiting Carbon Observatory-2 and 3 (OCO-2 and OCO-3): Data Product Users Guide, Operational Level 2 Data Versions 10
         and Lite File Version 10 and VEarly, 3, 2020.

Osterman, G. B., Eldering, A., Mandrake, L., O'Dell, C., Wunch, D., Wennberg, P. O., Fisher, B., and Marchetti, Y.: OCO-2 XCO2 V8r Lite
500   Products, Warn Levels, and Bias Correction, 2, https://docserver.gesdisc.eosdis.nasa.gov/public/project/OCO/OCO2_XCO2_Lite_Files_
         and_Bias_Correction.pdf, 2017.

Park, C., Jeong, S., Park, H., Yun, J., and Liu, J.: Evaluation of the Potential Use of Satellite-Derived XCO2 in Detecting CO2 Enhancement
         in Megacities with Limited Ground Observations: A Case Study in Seoul Using Orbiting Carbon Observatory-2, Asia-Pacific Journal of
         Atmospheric Sciences, 57, 289–299, https://doi.org/10.1007/s13143-020-00202-5, 2021.

505 Sha, M. K., Mazière, M. D., Notholt, J., Blumenstock, T., Chen, H., Dehn, A., Griffith, D. W. T., Hase, F., Heikkinen, P., Hermans, C.,
         Hoffmann, A., Huebner, M., Jones, N., Kivi, R., Langerock, B., Petri, C., Scolas, F., Tu, Q., and Weidmann, D.: Intercomparison of low-
         and high-resolution infrared spectrometers for ground-based solar remote sensing measurements of total column concentrations of CO2,
         CH4 and CO, Atmospheric Measurement Techniques, 13, 4791–4839, https://doi.org/10.5194/amt-13-4791-2020, 2020.

Shekhar, A., Chen, J., Paetzold, J. C., Dietrich, F., Zhao, X., Bhattacharjee, S., Ruisinger, V., and Wofsy, S. C.: Anthropogenic CO2
510   emissions assessment of Nile Delta using XCO2 and SIF data from OCO-2 satellite, Environmental Research Letters, 15, 095 010,
         https://doi.org/10.1088/1748-9326/ab9cfe, 2020.

Shukla, P., Skea, J., Buendia, E. C., Masson-Delmotte, V., Pörtner, H.-O., Roberts, D. C., Zhai, P., Slade, R., Connors, S., van Diemen,
         R., Ferrat, M., Haughey, E., Luz, S., Neogi, S., Pathak, M., adn J. Portugal Pereira, J. P., Vyas, P., Huntley, E., Kissick, K., Belkacemi,
         M., and Malley, J.: IPCC, 2019: Climate Change and Land: an IPCC special report on climate change, desertification, land degradation,
515   sustainable land management, food security, and greenhouse gas fluxes in terrestrial ecosystems, The Intergovernmental Panel on Climate
         Change, 2019.

Super, I., Dellaert, S. N. C., Visschedijk, A. J. H., and Denier van der Gon, H. A. C.: Uncertainty analysis of a European high-resolution emission inventory of CO_2 and CO to support inverse modelling and network design, Atmospheric Chemistry and Physics, 20, 1795–1816, https://doi.org/10.5194/acp-20-1795-2020, 2020.

520 Wu, C. and Zhen Yu, J.: Evaluation of linear regression techniques for atmospheric applications: The importance of appropriate weighting, Atmospheric Measurement Techniques, 11, 1233–1250, https://doi.org/10.5194/amt-11-1233-2018, 2018.

Wu, D., Lin, J., Fasoli, B., Oda, T., Ye, X., Lauvaux, T., Yang, E., and Kort, E.: A Lagrangian approach towards extracting signals of urban CO2 emissions from satellite observations of atmospheric column CO2 (XCO2): X-Stochastic Time-Inverted Lagrangian Transport model ("X-STILT v1"), Geoscientific Model Development, 11, 4843–4871, https://doi.org/10.5194/gmd-11-4843-2018, 2018.

525 Wu, L., Broquet, G., Ciais, P., Bellassen, V., Vogel, F., Chevallier, F., Xueref-Remy, I., and Wang, Y.: What would dense atmospheric observation networks bring to the quantification of city CO2 emissions?, Atmospheric Chemistry and Physics, 16, 7743–7771, https://doi.org/10.5194/acp-16-7743-2016, 2016.

Wunch, D., Toon, G. C., Blavier, J.-F. L., Washenfelder, R. A., Notholt, J., Connor, B. J., Griffith, D. W. T., Sherlock, V., and Wennberg, P. O.: The Total Carbon Column Observing Network, Philosophical Transactions of the Royal Society of London A: Mathematical, Physical

530 and Engineering Sciences, 369, 2087–2112, https://doi.org/10.1098/rsta.2010.0240, 2011.

Wunch, D., Wennberg, P. O., Osterman, G., Fisher, B., Naylor, B., Roehl, M. C., O'Dell, C., Mandrake, L., Viatte, C., Kiel, M., Griffith, D. W., Deutscher, N. M., Velazco, V. A., Notholt, J., Warneke, T., Petri, C., De Maziere, M., Sha, M. K., Sussmann, R., Rettinger, M., Pollard, D., Robinson, J., Morino, I., Uchino, O., Hase, F., Blumenstock, T., Feist, D. G., Arnold, S. G., Strong, K., Mendonca, J., Kivi, R., Heikkinen, P., Iraci, L., Podolske, J., Hillyard, P., Kawakami, S., Dubey, M. K., Parker, H. A., Sepulveda, E., García, O. E., Te, Y., Jeseck,

535 P., Gunson, M. R., Crisp, D., and Eldering, A.: Comparisons of the Orbiting Carbon Observatory-2 (OCO-2) XCO2 measurements with TCCON, Atmospheric Measurement Techniques, 10, 2209–2238, https://doi.org/10.5194/amt-10-2209-2017, 2017.

York, D., Evensen, N. M., Martinez, M. L., and Delgado, J. D. B.: Unified equations for the slope, intercept, and standard errors of the best straight line, American Journal of Physics, 72, 367–375, https://doi.org/10.1119/1.1632486, 2004.

Young, C. R.: User Manual: Model 61302 Barometric Pressure Sensor, 2801 Aero Park Drive, Traverse City, Michigan 49686 USA, 2009.

540 Zhao, X., Chen, J., Marshall, J., Galkowski, M., and Gerbig, C.: The semi-operational Multi-scale Modelling Infrastructure for Munich, pp. 1–10, https://doi.org/https://doi.org/10.5194/egusphere-egu2020-13164, 2020a.

Zhao, X., Chen, J., Marshall, J., Galkowski, M., Gerbig, C., Hachinger, S., Dietrich, F., Lan, L., Knote, C., and Gon, H. D. V. D.: A semi-operational near-real-time Modelling Infrastructure for assessing GHG emissions in Munich using WRF-GHG, pp. 2018–2019, 2020b.